




 Cite this: *RSC Adv.*, 2021, **11**, 25211

# Structures and conductivities of stable and metastable $\text{Li}_5\text{GaS}_4$ solid electrolytes

 Takuya Kimura, Chie Hotehama, Atsushi Sakuda,  Masahiro Tatsumisago and Akitoshi Hayashi \*

Understanding the differences in the structures and defects in the stable crystalline phase and metastable phase is important for increasing the ionic conductivities of a solid electrolyte. The metastable phase often has higher conductivity than the stable phase. In this study, metastable lithium thiogallate,  $\text{Li}_5\text{GaS}_4$ , was synthesized *via* mechanochemistry and stable  $\text{Li}_5\text{GaS}_4$  was obtained by heating the metastable phase. The metastable  $\text{Li}_5\text{GaS}_4$  sample was found to have an antifluorite-type crystal structure with cationic disorder, while the stable phase was found to have a monoclinic crystal structure, similar to that of another solid electrolyte,  $\text{Li}_5\text{AlS}_4$ . In both the structures, the  $\text{Ga}^{3+}$  cations were surrounded by four  $\text{S}^{2-}$  anions in tetrahedral coordination. The conductivity of the metastable phase was determined to be  $2.1 \times 10^{-5} \text{ S cm}^{-1}$  at  $25^\circ\text{C}$ , which is 1000 times greater than that of the monoclinic phase. The high conductivity of the metastable phase was achieved owing to cation disorder in the crystal structure.

 Received 24th April 2021  
 Accepted 9th July 2021

DOI: 10.1039/d1ra03194e

[rsc.li/rsc-advances](http://rsc.li/rsc-advances)

## Introduction

Solid electrolytes, one of the key materials for realizing all-solid-state batteries, are required to have high ionic conductivity, suitable deformability, and high chemical/electrochemical stability. A number of previous studies have suggested that sulfide-based electrolytes meet these requirements. In particular, the ionic conductivities of sulfide electrolytes reach  $10^{-2} \text{ S cm}^{-1}$  at  $25^\circ\text{C}$ , a value comparable to that of the organic liquid electrolytes used in commercial lithium-ion batteries.<sup>1,2</sup>

Moreover, sulfide electrolytes have better deformability for densification than oxide electrolytes.<sup>3</sup> So far, various sulfides, such as  $\text{Li}_2\text{S-P}_2\text{S}_5$  glass-based electrolytes,<sup>4-9</sup> thio-LISICON-type crystals,<sup>10-14</sup>  $\text{Li}_{10}\text{GeP}_2\text{S}_{12}$ -type crystals,<sup>1,2,15,16</sup> and argyrodite-type crystals,<sup>17-20</sup> have been reported as solid electrolytes. These solid electrolytes have been prepared with a wide range of compositions. For example, the thio-LISICON series have been prepared in the form of  $\text{Li}_4\text{GeS}_4\text{-Li}_3\text{PS}_4$ ,  $\text{Li}_4\text{GeS}_4\text{-Li}_5\text{GaS}_4$ ,  $\text{Li}_3\text{PS}_4\text{-Li}_4\text{SiS}_4$ , *etc.*<sup>12,14,21</sup> Further, the crystal structures and conductivities at room temperature of  $\text{Li}_4\text{GeS}_4$ ,  $\text{Li}_3\text{PS}_4$ , and  $\text{Li}_4\text{SiS}_4$ , which are the terminal compositions in binary systems, have been reported. As the other terminal composition,  $\text{Li}_5\text{GaS}_4$  has been reported to have a low conductivity of  $5.1 \times 10^{-8} \text{ S cm}^{-1}$  at  $100^\circ\text{C}$ ;<sup>14</sup> however, its crystal structure has not been reported. The  $\text{Li}_5\text{GaS}_4$  crystals are stable at room temperature and can be readily prepared by heating a mixture of the starting materials. On the other hand, glassy and amorphous

electrolytes are prepared by melt quenching or a mechanochemical process.<sup>4-8</sup> In general, glassy and amorphous electrolytes have higher conductivities than the corresponding crystalline phases, because of their higher free volumes. Such glasses are notable precursors for metastable superionic conductive crystals. For example, when the  $70\text{Li}_2\text{S}\cdot 30\text{P}_2\text{S}_5$  glass is heated to  $240^\circ\text{C}$ , the superionic conductive phase of  $\text{Li}_7\text{P}_3\text{S}_{11}$  precipitates as a metastable phase in the amorphous matrix.<sup>6,8,22</sup> In addition, metastable crystalline phases can be prepared directly *via* mechanochemistry,<sup>23,24</sup> and metastable crystalline phases often exhibit higher conductivities than the stable crystalline phases. For instance,  $\text{Li}_4\text{SnS}_4$  prepared by heating a mixture of the starting materials has a stable orthorhombic crystal structure,<sup>25,26</sup> while the  $\text{Li}_4\text{SnS}_4$  sample prepared by the mechanochemical process has the metastable hexagonal crystal structure.<sup>24</sup> Further, the metastable hexagonal  $\text{Li}_4\text{SnS}_4$  has higher ionic conductivity than the stable orthorhombic  $\text{Li}_4\text{SnS}_4$ .

In this study, we focused on the thio-LISICON composition of  $\text{Li}_5\text{GaS}_4$ , whose crystal structure has not yet been clarified. In particular, the formation of the metastable phase of  $\text{Li}_5\text{GaS}_4$  by a mechanochemical process (ball milling) was investigated. Subsequently, crystalline phases were obtained by heating the milled metastable  $\text{Li}_5\text{GaS}_4$  sample at different temperatures. The structures of the different crystalline phases were analyzed by X-ray diffraction (XRD) and Raman spectral analyses, and the conductivities of the stable and metastable phases were also examined.

## Experimental section

$\text{Li}_2\text{S}$  (Mitsuiwa Chemical Co., Ltd., 99.9%) and  $\text{Ga}_2\text{S}_3$  (Kojundo Chemical Lab. Co., Ltd., 99.99%) powders were used as the

Department of Applied Chemistry, Graduate School of Engineering, Osaka Prefecture University, 1-1 Gakuen-cho, Naka-ku, Sakai, Osaka 599-8531, Japan. E-mail: hayashi@chem.osakafu-u.ac.jp; Fax: +81-72-2549910; Tel: +81-72-2549334



starting materials for the mechanochemical synthesis of the  $\text{Li}_5\text{GaS}_4$  solid electrolytes. A stoichiometric mixture of  $5\text{Li}_2\text{S} \cdot 1\text{Ga}_2\text{S}_3$  ( $= \text{Li}_5\text{GaS}_4$ ) was mechanochemically processed at 510 rpm for 100 h using a planetary ball mill apparatus (Pulverisette 7; Fritsch GmbH). In this process, 0.5 g of the mixture of the starting materials was milled in a 45 mL zirconia pot with 250 zirconia balls (diameter: 4 mm). After the mechanochemical process, the  $\text{Li}_5\text{GaS}_4$  powder was collected; this sample is hereafter referred to as milled  $\text{Li}_5\text{GaS}_4$ . The milled powder was subsequently heated at 420 or 600 °C for 2 h in a dry argon atmosphere; the heat-treated  $\text{Li}_5\text{GaS}_4$  samples are referred to as HT-420 °C or HT-600 °C, respectively. All the steps in the synthesis were carried out in a dry argon atmosphere.

X-ray diffraction (XRD) of the powder was performed on an X-ray diffractometer (SmartLab, Rigaku Corporation) using  $\text{Cu-K}\alpha$  radiation. The diffraction patterns were obtained in steps of  $0.02^\circ$  in the  $2\theta$  range of  $10\text{--}80^\circ$  at a scan rate of  $10^\circ \text{ min}^{-1}$ . Rietveld refinement of the XRD patterns was performed using the RIETAN-FP software.<sup>27</sup> The diffraction data for the Rietveld refinement were collected in steps of  $0.02^\circ$  in the  $2\theta$  range of  $10\text{--}130^\circ$  at a scan rate of  $1^\circ \text{ min}^{-1}$  using monochromatic  $\text{Cu-K}\alpha_1$  radiation. For the Rietveld refinement, first, the peak shape, background coefficient, scale factor, and lattice constants were refined. Then, the occupancy was fixed at the stoichiometric composition, and the isotropic displacement parameters of sulfur and gallium were refined. The crystal models were obtained using the VESTA software.<sup>28</sup>

Raman spectroscopic analysis to identify the local structural units in the solid electrolytes was carried out using a Raman spectrophotometer (LabRAM HR-800, HORIBA Ltd.) equipped with a 532 nm diode-pumped solid-state laser.

The ionic conductivity of the solid electrolyte was determined through electrochemical impedance spectroscopy. The impedance data were obtained in the frequency range of  $10^7$  to  $10^{-1}$  Hz using an impedance analyzer (SI-1260, Solartron) at an applied AC voltage of 50 mV. The prepared electrolyte powders were pressed at 360 MPa to form pellets at room temperature ( $\sim 25^\circ \text{C}$ ). The diameter and thickness of the pellets were approximately 10 mm and 1 mm, respectively. Thin gold films were coated onto the entire surface of the pellets on both the sides to serve as current collectors. The ionic conductivity was measured in the temperature range of approximately  $30\text{--}75^\circ \text{C}$ . Activation energies ( $E_a$ ) were calculated from the slopes of the Arrhenius plots and then the conductivities at  $25^\circ \text{C}$  ( $\sigma_{25^\circ \text{C}}$ ) was obtained by extrapolation.

## Results

First, the solid electrolyte, milled  $\text{Li}_5\text{GaS}_4$  was prepared by a mechanochemical process. Then, the milled sample was heated at 420 or 600 °C to obtain heated samples (HT-420 °C or HT-600 °C). The milled and heat-treated samples were white powders. Fig. 1 shows the powder XRD patterns of the as-milled and heated  $\text{Li}_5\text{GaS}_4$  samples, along with those of the starting materials. The XRD patterns of the prepared  $\text{Li}_5\text{GaS}_4$  samples contain peaks of unknown phases, as indicated by blue circles or red stars (Fig. 1). The peaks marked by blue circles are similar to those of  $\text{Li}_2\text{S}$  with an antifluorite-type structure belonging to the cubic system. The XRD pattern of the milled sample only

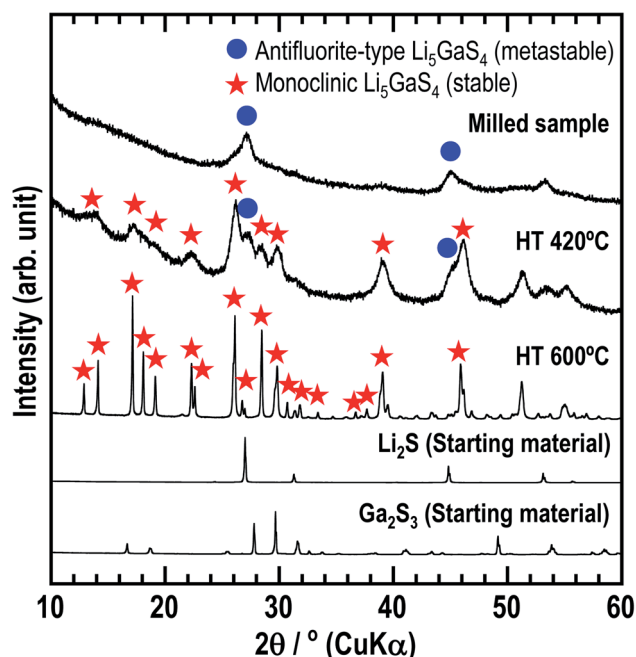


Fig. 1 XRD patterns of the three prepared  $\text{Li}_5\text{GaS}_4$  samples and starting materials ( $\text{Li}_2\text{S}$  and  $\text{Ga}_2\text{S}_3$ ). The milled sample was prepared by a mechanochemical process, while the HT samples were obtained by heating the milled sample at 420 or 600 °C. Blue circles and red stars indicate the peaks corresponding to the metastable cation-occupancy-disordered antifluorite-type structure and stable monoclinic structure, respectively.

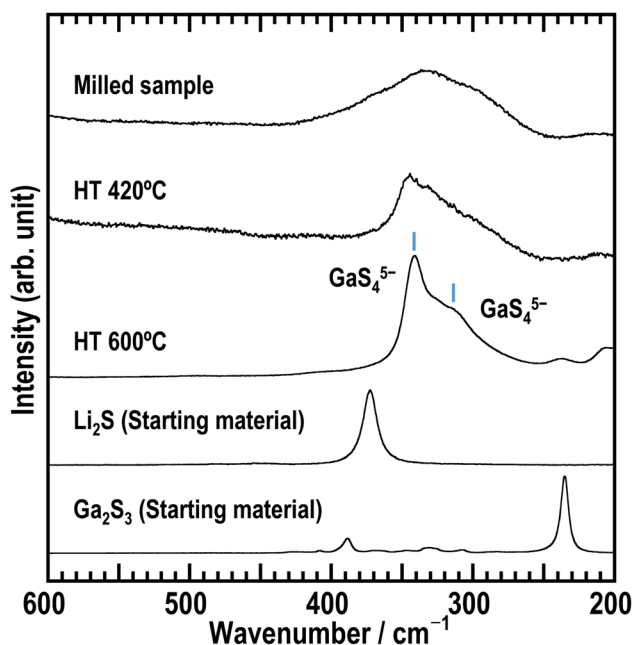


Fig. 2 Raman spectra of the three  $\text{Li}_5\text{GaS}_4$  samples and starting materials ( $\text{Li}_2\text{S}$  and  $\text{Ga}_2\text{S}_3$ ).



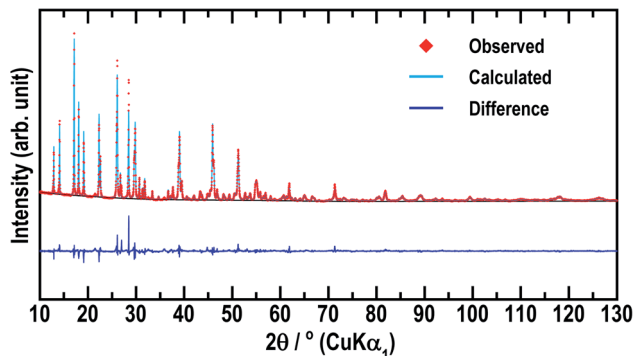


Fig. 3 Rietveld refinement of the X-ray diffraction data (Cu-K $\alpha_1$  radiation) for stable monoclinic Li<sub>5</sub>GaS<sub>4</sub>. The red rhombuses, pale blue line, and dark blue line indicate the observed intensity, calculated intensity, and intensity difference, respectively.

contains the set of peaks marked by blue circles. When the milled sample was heated at 420 °C, two sets of peaks (both the peaks marked by blue circles and by red stars) appeared in the XRD pattern. The peaks marked by red stars could be indexed to the monoclinic structure. Upon heating at a higher temperature of 600 °C, only the peaks marked by red stars were observed. Thus, as the heat-treatment temperature was increased, the peaks indexed to the cubic structure disappeared, while the peaks indexed to the monoclinic structure appeared. These results suggest that the cubic structure is the metastable phase, while the monoclinic structure is the stable phase.

Fig. 2 shows the Raman spectra of as-milled Li<sub>5</sub>GaS<sub>4</sub> and the heated samples. The spectrum of the milled sample shows a broad peak centered at  $\sim 335$  cm<sup>-1</sup>. This peak may contain multiple peaks, but the peak separation is difficult. The peak does not include the component of Ga<sub>2</sub>S<sub>3</sub> used as the starting material, because its main peak appears at a different wavenumber. Upon heating the sample, the Raman spectrum changed; an asymmetric peak appeared at  $\sim 345$  cm<sup>-1</sup> in the

spectrum of HT-420 °C, while two strong peaks appeared at  $\sim 310$  and  $340$  cm<sup>-1</sup> for HT-600 °C. Note that the bands at  $\sim 310$  and  $340$  cm<sup>-1</sup> have not been attributed to any units in glasses containing Ga<sub>2</sub>S<sub>3</sub> in previous studies.<sup>29,30</sup> Based on the X-ray crystal structure results of HT-600 °C, which will be discussed later, the Raman bands at  $310$  and  $340$  cm<sup>-1</sup> observed for HT-600 °C are assigned to isolated GaS<sub>4</sub> tetrahedral units.

To date, only the conductivity of Li<sub>5</sub>GaS<sub>4</sub> has been reported,<sup>14</sup> but not its crystal structure. Among the materials with the composition of 5Li<sub>2</sub>S·1M<sub>2</sub>S<sub>3</sub> (= Li<sub>5</sub>MS<sub>4</sub>; M = B, Al, Ga, In, and Tl), only the crystal structure of Li<sub>5</sub>AlS<sub>4</sub> has been analyzed in detail.<sup>13</sup> The similarity of the XRD patterns of Li<sub>5</sub>AlS<sub>4</sub> and Li<sub>5</sub>GaS<sub>4</sub> was exploited to identify the crystal structure of Li<sub>5</sub>GaS<sub>4</sub>. The Rietveld refinement results for Li<sub>5</sub>GaS<sub>4</sub> are presented in Fig. 3 and Table 1, and the crystal structure of Li<sub>5</sub>GaS<sub>4</sub> is shown in Fig. 4. Li<sub>5</sub>GaS<sub>4</sub> has the tetrahedral sites of lithium and gallium, and the octahedral site of lithium. In the Rietveld refinement of the XRD pattern of the HT-600 °C sample, the parameters reported for Li<sub>5</sub>AlS<sub>4</sub> (*P*<sub>2</sub><sub>1</sub>/*m* (space group No. 11), *a* = 6.2488 Å, *b* = 7.8369 Å, *c* = 6.8583 Å,  $\beta$  = 90.333°) were used as the initial structural parameters, and then the parameters were refined using the Le Bail method. In the Rietveld refinement, the occupancy of all atoms and the atomic displacement parameters of Li were not refined. The full profile and Rietveld fitting of Li<sub>5</sub>GaS<sub>4</sub> clearly reveal that the refined structure is almost accurate except for the difference in peak intensity at about 28°, which is probably due to the partial occupancy of gallium at the lithium site. Further analysis by neutron diffraction or single crystal X-ray diffraction is required to determine the lithium and gallium occupancy in detail.

Fig. 5 shows the temperature-dependence of the conductivities of the three Li<sub>5</sub>GaS<sub>4</sub> samples. At the composition of Li<sub>5</sub>GaS<sub>4</sub>, the conductivities differed according to the heating temperature. The milled sample showed the highest conductivity of  $2.2 \times 10^{-5}$  S cm<sup>-1</sup> at 25 °C among the three prepared samples. The ionic conductivities of HT-420 °C and HT-600 °C at 25 °C were  $8.1 \times 10^{-7}$  and  $2.1 \times 10^{-8}$  S cm<sup>-1</sup>, respectively.

Table 1 Crystallographic data of stable monoclinic Li<sub>5</sub>GaS<sub>4</sub> obtained by the Rietveld refinement of the X-ray (Cu-K $\alpha_1$  radiation) diffraction. Fractional coordinates and occupancies for Li<sub>5</sub>GaS<sub>4</sub>. *mW* denotes the integrated combination of the multiplicity and Wyckoff letter<sup>a</sup>

Crystal system		Monoclinic					
Space group		<i>P</i> <sub>2</sub> <sub>1</sub> / <i>m</i> (no. 11)					
Lattice parameter		<i>a</i> = 6.262 (1) Å, <i>b</i> = 7.857 (2) Å, <i>c</i> = 6.852 (2) Å, $\alpha = \gamma = 90^\circ$ , $\beta = 90.21 (1)^\circ$					
Volume		<i>V</i> = 337.135 (130) Å <sup>3</sup> , <i>Z</i> = 2					
Site	<i>mW</i>	<i>x</i>	<i>y</i>	<i>z</i>	Occ.	<i>U</i> Å <sup>-2</sup>	
S1	2 <i>e</i>	0.7539 (5)	1/4	0.8549 (6)	1	0.0120 (15)	
S2	2 <i>e</i>	0.2651 (5)	1/4	0.1749 (6)	1	0.0042 (11)	
S3	4 <i>f</i>	0.7557 (3)	0.0101 (3)	0.3322 (4)	1	0.0096 (9)	
Ga	2 <i>e</i>	0.6326 (3)	1/4	0.1706 (3)	1	0.0087 (7)	
Li1	4 <i>f</i>	0.3515 (28)	0.5167 (16)	0.3290 (27)	1	0.0127	
Li2	2 <i>e</i>	0.3524 (45)	1/4	0.8413 (44)	1	0.0127	
Li3	2 <i>e</i>	0.0008 (40)	1/4	0.4967 (36)	1	0.0127	
Li4	2 <i>a</i>	0	0	0	1	0.0127	

<sup>a</sup>  $R_{wp} = 9.370$ ,  $R_F = 1.162$ ,  $R_B = 3.676$ ,  $S = R_{wp}/R_e = 2.4003$ .



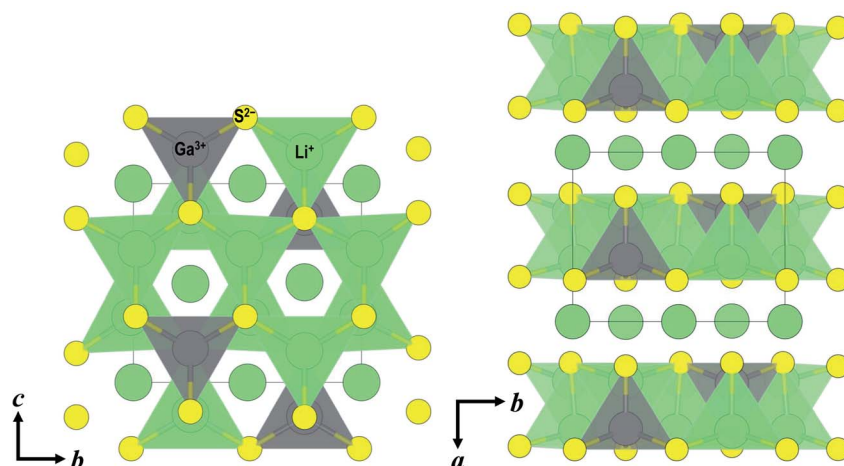


Fig. 4 Crystal structures of monoclinic  $\text{Li}_5\text{GaS}_4$  viewed along the  $a$ -axis (left) and along the  $c$ -axis (right). Each tetrahedron includes either a lithium or gallium atom in the central position. Lithium atoms in the octahedral interstices are represented by spheres. Green, gray, and yellow spheres represent lithium, gallium, and sulfur, respectively.

The activation energies of the milled sample, HT-420 °C, and HT-600 °C were calculated to be 37, 44, and 47  $\text{kJ mol}^{-1}$ , respectively.

## Discussion

In the XRD patterns of the prepared  $\text{Li}_5\text{GaS}_4$  samples (Fig. 1), the peaks of the milled sample are comparable to those of  $\text{Li}_2\text{S}$ , one of the two starting material. However, the Raman band of

crystalline  $\text{Li}_2\text{S}$  at  $\sim 370 \text{ cm}^{-1}$  was not clearly observed in the Raman spectrum of the milled  $\text{Li}_5\text{GaS}_4$  sample. Thus, the peaks marked by blue circles in the XRD patterns were assigned to the antifluorite-type crystal structure, and not to the starting material  $\text{Li}_2\text{S}$ . Although a detailed analysis of the metastable crystal phase is difficult because of the broad XRD peaks, the observed XRD peaks can be attributed to a new metastable phase with the antifluorite-type crystal structure, which has eight tetrahedral sites for the cation surrounded by four anions in a unit cell. In general, in a cation-disordered crystal structure, the cation sites are randomly occupied by cations or defects. In the case of antifluorite-type  $\text{Li}_5\text{GaS}_4$ , lithium cations, gallium cations, and defects randomly occupy the eight cation sites. The metastable antifluorite-type  $\text{Li}_5\text{GaS}_4$  has a similar structure to the monoclinic  $\text{Li}_5\text{GaS}_4$  (Fig. 4) because both phases are composed of isolated  $\text{GaS}_4$  tetrahedra. The ionic radii of lithium and gallium cations in the antifluorite-type crystal are however significantly different; the sizes of  $\text{Li}^+$  and  $\text{Ga}^{3+}$  are 0.59 Å and 0.47 Å under tetrahedral coordination ( $n = 4$ ;  $n$  is the coordination number), respectively.<sup>31</sup> The cation sites of the antifluorite-type structure seem to have a high tolerance to the size of the cations. Such a cation-disordered phase has been previously reported for  $\text{Li}_4\text{SnS}_4$  and  $\text{Li}_2\text{TiS}_3$ .<sup>24,32</sup> In the crystal structure of hexagonal  $\text{Li}_4\text{SnS}_4$ , the tetrahedral sites are occupied by  $\text{Li}^+$  ( $r_{\text{ionic}}(n = 4)$ : 0.59 Å) and  $\text{Sn}^{4+}$  ( $r_{\text{ionic}}(n = 4)$ : 0.55 Å). In the mechanochemically synthesized  $\text{Li}_2\text{TiS}_3$ , the octahedral sites are occupied by cations of different sizes, *viz.*,  $\text{Li}^+$  ( $r_{\text{ionic}}(n = 6)$ : 0.76 Å) and  $\text{Ti}^{4+}$  ( $r_{\text{ionic}}(n = 6)$ : 0.605 Å). These results indicate that cation disorder is possible not only in a structure with cations of similar sizes but also in structures containing cations of different sizes prepared by the mechanochemical process. Thus, the mechanochemical process is effective in the preparation of disordered structures, and the obtained disordered structures are metastable and have faster ionic conduction than the thermodynamically stable phases. The milled  $\text{Li}_5\text{GaS}_4$  sample with a metastable crystal structure has higher

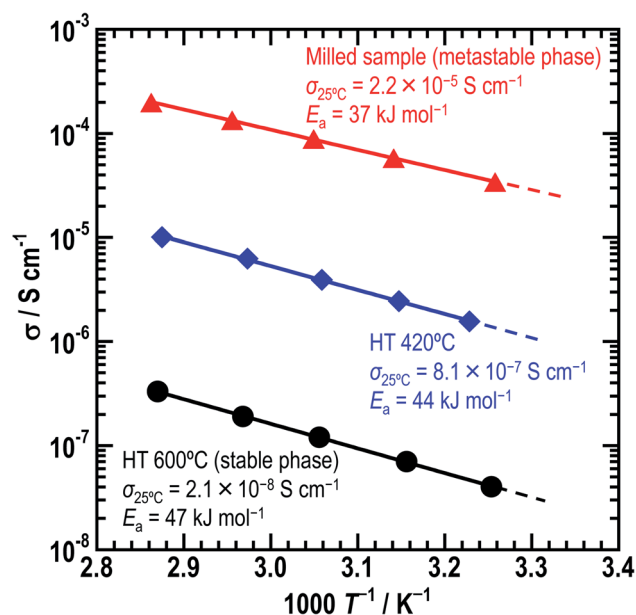


Fig. 5 Temperature-dependence of the conductivities of the three  $\text{Li}_5\text{GaS}_4$  samples. Red triangles, blue rhombuses, and black circles indicate the conductivities of the milled, HT-420 °C, and HT-600 °C samples, respectively. The activation energies were calculated using the Arrhenius equation,  $\sigma = A \exp(-E_a/RT)$ , where  $A$ ,  $\sigma$ ,  $E_a$ ,  $R$ , and  $T$  are the pre-exponential factor, conductivity, activation energy, gas constant, and measurement temperature, respectively.



conductivity ( $2.2 \times 10^{-5} \text{ S cm}^{-1}$ ) than the heated samples with a stable crystal structure ( $2.1 \times 10^{-8} \text{ S cm}^{-1}$ ) at 25 °C, as shown in Fig. 5. The XRD peaks attributable to the metastable phase in the milled  $\text{Li}_5\text{GaS}_4$  sample are broad, and they are mainly due to small crystallite size and/or disordered structure of the metastable phase. The sample possibly includes amorphous phase, which may contribute to the high conductivity of the milled  $\text{Li}_5\text{GaS}_4$  sample.

In the structural analysis of the stable  $\text{Li}_5\text{GaS}_4$  crystal, the structural parameters were refined using the parameters of  $\text{Li}_5\text{AlS}_4$ . The lattice volumes of  $\text{Li}_5\text{GaS}_4$  and  $\text{Li}_5\text{AlS}_4$  are 337.135 and 335.8537 Å<sup>3</sup>, respectively. Although the difference between the cation radii of  $\text{Ga}^{3+}$  (0.47 Å) and  $\text{Al}^{3+}$  (0.39 Å)<sup>31</sup> for tetrahedral coordination is large, the difference in their volumes is small. This assumption is reasonable considering the packed structure of the anions and cations. If we consider the ions as rigid spheres for simplicity, the critical ionic radius ratio for tetrahedral coordination ( $r_{\text{cation}}/r_{\text{anion}}$ ) is 0.225. In the  $\text{MS}_4$  tetrahedral unit, the critical cation radius is 0.41 Å, when the anion radius of  $\text{S}^{2-}$  is 1.84 Å.<sup>31</sup> The critical cation radius is larger than the radius of  $\text{Al}^{3+}$ , and the tetrahedral structure of  $\text{AlS}_4$  is unstable, according to simple numerical calculations. However, in fact, the tetrahedral unit is formed because of the distortion of the tetrahedral symmetry and the distortion of the electron clouds of the sulfide anions. The Ga–S and Al–S distances are 2.31 and 2.28 Å in the same tetrahedral unit, respectively. The volume of  $\text{GaS}_4$  tetrahedra is 6.34 Å<sup>3</sup>, larger than that of  $\text{AlS}_4$  tetrahedra (6.04 Å<sup>3</sup>). The crystal structure of  $\text{Li}_5\text{GaS}_4$  is illustrated in Fig. 4. The filling structure of the polyhedra ( $\text{GaS}_4$ ,  $\text{LiS}_4$ , and  $\text{LiS}_6$ ) in  $\text{Li}_5\text{GaS}_4$  is the same as that in  $\text{Li}_5\text{AlS}_4$ . The crystal of  $\text{Li}_5\text{GaS}_4$  consists of two layers, the  $\text{MS}_4$  ( $M = \text{Li, Ga}$ ) layer and  $\text{LiS}_6$  layer, which are stacked alternately. All the tetrahedral interstices are occupied by Li or Ga in the  $\text{MS}_4$  layer, while all the octahedral interstices are occupied by Li in the  $\text{LiS}_6$  layer. In these crystals with completely filled sites, the ionic conductivity is usually low.

In crystalline ionic conductors, the site vacancy and number of carriers are important for fast ionic conduction. Considering the ionic conduction in the crystal structure, monoclinic  $\text{Li}_5\text{GaS}_4$  simultaneously has the advantage of high lithium content and the disadvantage of fully occupied sites. The conductivity of  $\text{Li}_5\text{GaS}_4$  HT-600 °C is  $2.1 \times 10^{-8} \text{ S cm}^{-1}$  at 25 °C. Note that  $\text{Li}_5\text{GaS}_4$  has been previously reported to have a low conductivity of  $5 \times 10^{-8} \text{ S cm}^{-1}$  at 100 °C.<sup>14</sup> In comparison, the conductivity of HT-600 °C (monoclinic) at 100 °C, as estimated using the Arrhenius equation, is ~20 times higher at  $9.8 \times 10^{-7} \text{ S cm}^{-1}$ .<sup>14</sup> Compared to those of other stoichiometric thio-LISICON materials, the conductivity of monoclinic  $\text{Li}_5\text{GaS}_4$  is lower; for instance, it is lower than those of  $\gamma\text{-Li}_3\text{PS}_4$  ( $3 \times 10^{-7} \text{ S cm}^{-1}$ ),<sup>10</sup>  $\text{Li}_4\text{SiS}_4$  ( $5 \times 10^{-8} \text{ S cm}^{-1}$ ),<sup>11</sup>  $\text{Li}_4\text{GeS}_4$  ( $3 \times 10^{-7} \text{ S cm}^{-1}$ ),<sup>14</sup> and  $\text{Li}_4\text{SnS}_4$  ( $7 \times 10^{-5} \text{ S cm}^{-1}$ ),<sup>25</sup> but higher than those of  $\text{Li}_5\text{AlS}_4$  ( $9.7 \times 10^{-9} \text{ S cm}^{-1}$  at 50 °C)<sup>13</sup> and  $\text{Li}_3\text{SbS}_4$  ( $4.8 \times 10^{-9} \text{ S cm}^{-1}$ ).<sup>33</sup> The differences in the conductivities is due to the lithium content, vacancy of lithium sites, and central cation–sulfide anion interaction. Understanding the differences in the conductivities of thio-LISICON is challenging because of various factors, such as the differences in their ductility and

relative density of pellets. The HT-420 °C sample, which has a mixed structure consisting of the antifluorite-type and monoclinic crystals, shows a conductivity of  $8.1 \times 10^{-7} \text{ S cm}^{-1}$ , which is higher than that of HT-600 °C. This results from the precipitation of the metastable phase. Thus, among the three samples prepared in this study, the as-milled sample with the metastable antifluorite-type crystal phase has the highest conductivity, while the HT-600 °C sample with the stable monoclinic crystal phase has the lowest conductivity. The results clearly indicate that the antifluorite-type crystal is more suitable for ionic conduction than the monoclinic crystal.

## Conclusions

In this study, sulfide antifluorite-type structure is proposed as a new framework for ionic conduction. A metastable  $\text{Li}_5\text{GaS}_4$  solid electrolyte was prepared by a mechanochemical process and subsequently transformed into a stable  $\text{Li}_5\text{GaS}_4$  solid electrolyte by heat treatment. The mechanochemically processed sample had the metastable antifluorite-type phase. When heated at 600 °C, the phase transformed to the stable monoclinic one, similar to that of  $\text{Li}_5\text{AlS}_4$ . The conductivity of the milled sample (metastable antifluorite-type phase) was determined to be  $2.1 \times 10^{-5} \text{ S cm}^{-1}$  at 25 °C, which is three orders of magnitude higher than that of the heated sample with the stable phase. Thus, it is concluded that the metastable phase is a more suitable structure for ionic conduction than the stable phase at the composition of  $\text{Li}_5\text{GaS}_4$ . The results of this study extend research toward understanding sulfide electrolytes with cation-disordered metastable phases and cation-ordered stable phases, and contribute to the development of solid electrolytes with high ionic conductivity.

## Author contributions

T. K., A. S., and A. H. designed the experiments and wrote the paper. T. K. synthesized and characterized the electrolytes. T. K. and C. H. performed the crystal analysis. A. S., T. M., and A. H. supervised the study. All of the authors discussed the results and commented on the manuscript.

## Conflicts of interest

There are no conflicts to declare.

## Acknowledgements

This research was financially supported by the JSPS Grant-in-Aid for Scientific Research on Innovative Areas “Mixed anion” (17H05488).

## References

- N. Kamaya, K. Homma, Y. Yamakawa, M. Hirayama, R. Kanno, M. Yonemura, T. Kamiyama, Y. Kato, S. Hama, K. Kawamoto and A. Mitsui, *Nat. Mater.*, 2011, **10**, 682–686.



- 2 Y. Kato, S. Hori, T. Saito, K. Suzuki, M. Hirayama, A. Mitsui, M. Yonemura, H. Iba and R. Kanno, *Nat. Energy*, 2016, **1**, 16030.
- 3 A. Sakuda, A. Hayashi and M. Tatsumisago, *Sci. Rep.*, 2013, **3**, 2261.
- 4 A. Hayashi, S. Hama, H. Morimoto, M. Tatsumisago and T. Minami, *Chem. Lett.*, 2001, **30**, 872–873.
- 5 A. Hayashi, S. Hama, H. Morimoto, M. Tatsumisago and T. Minami, *J. Am. Ceram. Soc.*, 2004, **84**, 477–479.
- 6 F. Mizuno, A. Hayashi, K. Tadanaga and M. Tatsumisago, *Adv. Mater.*, 2005, **17**, 918–921.
- 7 Y. Seino, T. Ota, K. Takada, A. Hayashi and M. Tatsumisago, *Energy Environ. Sci.*, 2014, **7**, 627–631.
- 8 F. Mizuno, A. Hayashi, K. Tadanaga and M. Tatsumisago, *Solid State Ionics*, 2006, **177**, 2721–2725.
- 9 Z. Ma, H.-G. Xue and S.-P. Guo, *J. Mater. Sci.*, 2018, **53**, 3927–3938.
- 10 M. Tachez, J. P. Malugani, R. Mercier and G. Robert, *Solid State Ionics*, 1984, **14**, 181–185.
- 11 B. T. Ahn and R. A. Huggins, *Mater. Res. Bull.*, 1989, **24**, 889–897.
- 12 M. Murayama, R. Kanno, M. Irie, S. Ito, T. Hata, N. Sonoyama and Y. Kawamoto, *J. Solid State Chem.*, 2002, **168**, 140–148.
- 13 H. Lim, S.-C. Kim, J. Kim, Y.-I. Kim and S.-J. Kim, *J. Solid State Chem.*, 2018, **257**, 19–25.
- 14 R. Kanno, T. Hata, Y. Kawamoto and M. Irie, *Solid State Ionics*, 2000, **130**, 97–104.
- 15 S. Hori, K. Suzuki, M. Hirayama, Y. Kato and R. Kanno, *Front. Energy Res.*, 2016, **4**, 38.
- 16 Y. Sun, K. Suzuki, S. Hori, M. Hirayama and R. Kanno, *Chem. Mater.*, 2017, **29**, 5858–5864.
- 17 R. P. Rao and S. Adams, *Phys. Status Solidi A*, 2011, **208**, 1804–1807.
- 18 P. Adeli, J. D. Bazak, K. H. Park, I. Kochetkov, A. Huq, G. R. Goward and L. F. Nazar, *Angew. Chem., Int. Ed.*, 2019, **58**, 8681–8686.
- 19 M. A. Kraft, S. Ohno, T. Zinkevich, R. Koerver, S. P. Culver, T. Fuchs, A. Senyshyn, S. Indris, B. J. Morgan and W. G. Zeier, *J. Am. Chem. Soc.*, 2018, **140**, 16330–16339.
- 20 S. Ohno, B. Helm, T. Fuchs, G. Dewald, M. A. Kraft, S. P. Culver, A. Senyshyn and W. G. Zeier, *Chem. Mater.*, 2019, **31**, 4936–4944.
- 21 R. Kanno and M. Murayama, *J. Electrochem. Soc.*, 2001, **148**, 742–746.
- 22 F. Mizuno, A. Hayashi, K. Tadanaga and M. Tatsumisago, *Electrochem. Solid-State Lett.*, 2005, **8**, A603.
- 23 A. Hayashi, K. Noi, N. Tanibata, M. Nagao and M. Tatsumisago, *J. Power Sources*, 2014, **258**, 420–423.
- 24 K. Kanazawa, S. Yubuchi, C. Hotehama, M. Otoyama, S. Shimono, H. Ishibashi, Y. Kubota, A. Sakuda, A. Hayashi and M. Tatsumisago, *Inorg. Chem.*, 2018, **57**, 9925–9930.
- 25 T. Kaib, S. Haddadpour, M. Kapitein, P. Bron, C. Schröder, H. Eckert, B. Roling and S. Dehnen, *Chem. Mater.*, 2012, **24**, 2211–2219.
- 26 G. Sahu, Z. Lin, J. Li, Z. Liu, N. Dudney and C. Liang, *Energy Environ. Sci.*, 2014, **7**, 1053–1058.
- 27 F. Izumi and K. Momma, *Solid State Phenom.*, 2007, **130**, 15–20.
- 28 K. Momma and F. Izumi, *J. Appl. Crystallogr.*, 2011, **44**, 1272–1276.
- 29 T. Ishibashi, H. Takebe and K. Morinaga, *J. Ceram. Soc. Jpn.*, 2003, **111**, 308–311.
- 30 S. Barnier, M. Palazzi, M. Massot and C. Julien, *Solid State Ionics*, 1990, **44**, 81–86.
- 31 R. D. Shannon, *Acta Cryst. A*, 1976, **32**, 751–767.
- 32 A. Sakuda, T. Takeuchi, K. Okamura, H. Kobayashi, H. Sakaebe, K. Tatsumi and Z. Ogumi, *Sci. Rep.*, 2014, **4**, 4883.
- 33 T. Kimura, A. Kato, C. Hotehama, A. Sakuda, A. Hayashi and M. Tatsumisago, *Solid State Ionics*, 2019, **333**, 45–49.

